Spin-Coated Amino-Terminated Monolayers to Immobilize Gold Nanorods for SERS Detection of Biomolecules

Axelle Hachin,[a] Thierry Buffeteau,[a] Julien Hunel,[a] Jean-Paul Salvetat,[d] Yoann Roupioz,[e] Sébastien Bonhommeau,[a] Stéphane Mornet,[c] Mona Treguer-Delapierre,[c] Vincent Humblot[b]* Luc Vellutini[a]*

a. Univ. Bordeaux, CNRS, Bordeaux INP, ISM, UMR 5255, F-33400 Talence, France

b. Université Louis et Marie Pasteur, FEMTO-ST Institute, UMR CNRS 6174, 15B avenue des Montboucons, 25030 Besançon Cedex, France.

c. Placamat, CNRS, Université de Bordeaux, UAR3626, F-33600 Pessac, France

d. Univ. Grenoble Alpes, CNRS, CEA, Grenoble-INP, IRIG, SyMMES, F-38000 Grenoble, France

e. Univ. Bordeaux, CNRS, Bordeaux INP, ICMCB, UMR 5026, F-33600 Pessac, France

Abstract:

Silane-based Self-Assembled Monolayers (SAMs) are widely used to control the surface properties of materials. The spin coating technique is an interesting alternative way to the conventional immersion solution for organosilane deposition owing to its speed and ease of use under ambient conditions. In this work, we study the impact of the drying step following organosilane deposition by spin coating. We investigated the influence of temperature and time of the drying step on the quality of the monolayers. Two trimethoxysilanes bearing phthalimide end group with an alkyl chain or a urea moiety as spacer were used to prepare amino-terminated SAMs. The structural information of SAMs were provided by polarization modulation infrared reflection-adsorption spectroscopy (PM-IRRAS), time-of-flight secondary-ion mass spectrometry (ToF-SIMS) and X-ray photoelectron spectroscopy (XPS). Results showed that the urea group which induced self-assembly by intermolecular hydrogen bonding reduced the drying step time by half compared with the alkyl chain. Amino-terminated SAMs were derivatized to afford thiol-terminated SAMs to immobilize gold nanorods and constitute surface-enhanced Raman scattering (SERS) substrate. An oligonucleotide bearing a terminal thiol immobilized on gold nanorods was identified by SERS highlighting the potential of this SERS platform to be used as biosensors in the future.

1. Introduction

Self-Assembled Monolayers (SAMs) have emerged as versatile and tunable molecular platforms for a wide range of applications, including antifouling,[1] tribological applications,[2] batteries,[3] electronic[4] and plasmonic[5] devices, biosensors,[6] and the study of biological systems.[7]

Silane based SAMs are widely used to modify the properties of oxide surfaces.[8] These monolayers are prepared from organosilanes bearing a trichlorosilane or alkoxysilane as an anchoring group. A wide range of functionalities can be introduced on the surface using silanes carrying different functional groups such as ester,[9,10] alkene,[11,12] epoxide,[13,14] azide,[15,16] etc. These SAMs are generally stable and robust due to their partial in plane polymerization, offering long-term durability under a variety of environmental conditions. After formation,

SAMs can be easily modified by subsequent chemical treatment providing additional flexibility for surface design.[17]

The functionalization of silica surfaces with 3-aminopropyltriethoxysilane (APTES) or 3-aminopropyltrimethoxysilane (APTMS) has garnered significant attention for the development of biosensors.[6] These aminosilanes provide a reactive interface for the attachment of biomolecules, such as antibodies, enzymes, and DNA probes, enabling the detection of various analytes. One drawback of aminopropylsilanes layers was their instability which can lead to a desorption under physiological conditions.[18,19] This behavior comes from the formation of polycondensates in solution by homo-condensation reaction and from their surface physisorption which predominates over surface grafting by hetero-condensation reaction involving the silanol groups.[20] The disordered organization of the silane in the layer is the result of multiple possibilities of interactions of the terminal amino group by hydrogen bonds or electrostatic interactions, which can limit its accessibility and reactivity. These limitations render difficult the preparation of single monolayers of aminopropylsilanes, and rather favor multilayer formation.[21]

In contrast to commercial aminosilanes grafted by an immersion solution method, an alternative strategy using direct grafting of aminosilanes with phthalimide as a protecting amino group has demonstrated its efficiency to prepare a well-defined amino-terminated monolayer.[22,23,24] N-phthalimide protected aminosilanes avoid multiple interactions of the amine group, ensuring better control of the assembly during the grafting process, and therefore the molecular organization in the SAM, leading to the terminal group being directed outwards. The phthalimide-terminated SAMs can be prepared by using the classic immersion solution method or by spin coating. The latter offers the advantage of rapid silane deposition on the surface, easy operation under ambient conditions, and requires only a small amount of organic solvent. Recently, our research group investigated the possibility to prepare by spin coating SAMs based on trimethoxysilanes with different end groups like azide, bromine, benzyl and phthalimide.[16,25] All these SAMs were prepared under ambient atmosphere in two steps: (i) the fast deposition of the silane solution on the surface by spin coating, and (ii) the drying step at room temperature (RT) for a duration from 30 min to 14 hrs, depending on the molecular structure. Since this drying step can last several hours, the grafting process is just as long as the conventional immersion method. Heat treatment can accelerate the process by promoting polymerization of the silane in the layer.[26,27,21]

In this study, we have investigated the influence of temperature and time on the quality of phthalimide-terminated SAMs prepared by spin coating. Two phthalimide trimethoxysilanes bearing an alkyl chain or an urea group as a spacer were grafted on silica. After defining the optimum temperature and time for the drying step, the monolayers were deprotected to produce amino-terminated SAMs. To demonstrate the reactivity of free amine, these monolayers were modified by a bifunctional heterolinker to afford the corresponding thiol-terminated SAMs. The modified surfaces were characterized using polarization modulation infrared reflection-adsorption spectroscopy (PM-IRRAS), time-of-flight secondary-ion mass spectrometry (ToF-SIMS) and X-ray photoelectron spectroscopy (XPS) for interfacial reactivity, elemental composition and thickness. Wettability was measured with a contact angle goniometer and topography by atomic force microscopy (AFM).

Besides the preparation and characterization of SAMs at each step of the surface modification, gold nanorods (GNRs) were grafted onto them and an oligonucleotide was subsequently

immobilized on the SAM-GNR system to assess its potential use as SERS platform for the detection of biomolecules. Gold nanoparticles are indeed attractive functional building blocks to prepare nanostructured materials in plasmonics and sensors applications.[28,] This proof-of-concept study shows that silane-based synthetic routes are promising for the design of plasmonic devices, and especially SERS-active substrates.

2. Experimental

2.1. Materials and substrates

For PM-IRRAS experiments, SiO_2/Au substrates corresponding to Goldflex mirror with SiO_2 protection layer (Goldflex PRO, 5 × 5 cm, reference 200785), supplied by Optics Balzers AG, were used with a root-mean-square (rms) roughness of 0.9 nm. They are cut to 2.5 × 2.5 cm slides. The thickness of the SiO_2 layer was measured by ellipsometry and a value of 215 ± 7 Å was obtained, applying a refractive index of 1.46 (I-elli2000 NFT ellipsometer, λ = 532 nm). For AFM and ToF-SIMS experiments, silicon wafers measuring 1 cm × 1 cm (silicon-CZ undoped from BT Electronics) were used with a rms roughness of 0.2 nm.

2.2. Chemical surface modification

Substrate cleaning procedure: Before grafting, the substrates were intensively washed with Milli-Q water (18 MΩ cm), sonicated for 15 min in chloroform and exposed to UV- ozone (185 - 254 nm) for 30 min. They were immediately used for silanization by spin coating.

Preparation of phthalimide-terminated SAMs by spin coating: Freshly prepared organosilane was dissolved in anhydrous chloroform under inert atmosphere to prepare a solution at 4.10^{-3} M. A drop (40 µL for PM-IRRAS substrate and 15 µL for silicon wafer) of this organosilane solution was deposited on the substrate during the rotation (Spincoat G3P-8: 6000 rpm for 40 sec). Different time and temperature were applied for the drying step: at RT (20-25°C) at ambient humidity (30-40%) and at 100°C in an oven. The dry silanized substrate was then washed by sonication in chloroform (2 × 5 min), Milli-Q water (2 × 5 min) and chloroform again (2 × 5 min), and dried under nitrogen flow.

Deprotection of phthalimide groups: Amino-terminated SAMs were prepared following a protocol described in the literature.[28]

Thiol-terminated SAMs:

A drop (350 µL/3.6 mM) of 3-Mercaptopropanyl-N-hydroxysuccinimide ester (MPH) solution in anhydrous DMF was deposited on freshly deprotected amino-terminated SAMs, and incubated for 65 hrs at RT under argon and protected from light without stirring. After reaction, the substrates were washed in an ultrasonic bath for 2 × 5 min successively in DMF, Milli-Q water water, and chloroform, and finally dried under nitrogen flow.

Synthesis of GNRs: Colloidal GNRs were synthesized using a one-stage protocol (seedless approach).[29] 12 mL of an aqueous solution of CTAB (cetyltrimethylammonium bromide, Sigma-Aldrich) (200 mM) and 3.75 mL of NaOL (sodium oleate, TCI) (200 mM) were poured into 9.25 mL of Milli-Q water in a 200 mL glass vial. The solution was stirred at 150 rpm for a 1 cm cylindrical magnetic stirrer. When the temperature had stabilized at 30°C, 25 mL $HAuCl_4$ (gold chloride trihydrate, Sigma-Aldrich) (1 mM), 1.2 mL $AgNO_3$ (silver nitrate, Sigma-Aldrich) (4 mM), 250 µL HCl (11.8 M), and 375 µM ascorbic acid (85.8 mM) were added sequentially. 37.5 µL freshly prepared ice-cold $NaBH_4$ (sodium borohydride, Sigma-Aldrich) (10 mM) was then rapidly injected into the mixture. The solution was then immediately left

unstirred for 4 hrs at 30°C. AuNRs were then isolated by centrifugation at 9000 g for 30 minutes. The supernatant was discarded and the precipitate resuspended in Milli-Q and stored at room temperature. The sample was characterized by absorption spectroscopy and TEM. The shape yield is high as shown in Figure S6. Rods are formed with a morphology yield of 95%.The absorption spectrum shows well-defined longitudinal and transversal LSPR bands at 744 nm and 520 nm respectively. The average diameter and length of the as-obtained nano-objets were estimated to 76 ± 9 nm and 26 ± 4 nm respectively.

Surface modification of GNRs with PVP:
The excess of CTAB of freshly synthesized Nanorods solution (9.10^{14} GNRs / 250 µL) was removed by a double centrifugation (8600 rpm (4100g)/ 15 min), discarding the supernatant and redispersing the nanoparticles in Milli-Q water to have 250 µL of nanorod solution (9.10^{14} NP/L). A large excess (500 µL at 5 mM) of poly(vinyl-pyrrolidone) (PVP : 10 000 g/mol) was added to the CTAB-stabilized GNR solution and the PVP was allowed to adsorb onto the GNRs overnight under stirring at room temperature. Excess of PVP was removed by a double centrifugation (8600 rpm / 15 min), and the GNRs were redispersed in 500 µL Milli-Q water.

Immobilization of PVP-stabilized GNRs on SAMs:

SAM-Urea-SH and SAM-Urea-NH_2 were immersed in a solution containing 2.1 mL degassed Milli-Q water, 400 µL of TCEP (1 mM) and 500 µL of colloidal GNR solution (9.10^{11} NP/L). The substrate was stirred by orbital shaking (≈180 rpm) overnight at RT, under argon and protected from light. The substrate was washed in an ultrasonic bath using successively Milli-Q water, ethanol, and chloroform for 2 x 5 min, and then dried under nitrogen flow. All non-specific adhesion tests used the same protocols without the TCEP.

Immobilization of oligonucleotide (DNA strand) on nanorods-terminated SAMs:
A 150 µL drop of DNA strand solution in Milli-Q water (1.91 nmol DNA strand) containing 10 µL of TCEP (1 mM) was deposited on the surface and incubated for 65 h at RT without stirring, under argon and protected from light. The substrate was washed by a flow of Milli-Q water for 5 min and dried under nitrogen flow. Oligonucleotides were ordered from GeneCust (Boynes, France). The sequence of the DNA strand was 5'- Thiol-C6-TTT TTT TTT TAG TCC GTG GTA GGG CAG GTT GGG GTG ACT -3' and was resuspended in Milli-Q water and used without further purification.

2.3. Characterization of monolayers

PM-IRRAS analysis. PM-IRRAS experiments were performed on a FTIR spectrometer equipped with a PM-IRRAS optical bench, following the experimental procedure previously published.[30] The PM-IRRAS spectra were recorded at a 4 cm^{-1} spectral resolution for 4 h acquisition time. The PM-IRRAS spectra were calibrated in order to be presented in IRRAS units (i.e. 1-Rp(d)/Rp(0), where Rp(d) and Rp(0) stand for the p-polarized reflectance of the film/substrate and bare substrate systems, respectively). All spectra were collected in a dry-air atmosphere, after 30 min of incubation in the chamber.

AFM measurements. AFM height images of SAMs were performed on a Bruker's Dimension Icon Atomic Force Microscope (AFM) System in PeakForce QNM® mode (Quantitative Nanomechanical Mapping) with ScanAsyst-Air tips (apex diameter = 2 nm, spring constant k = 0.4 N/m). The AFM height images are representative of three different areas.

Wettability measurements. Contact angles were determined on a Krüss DSA 100 goniometer at 20 °C in static mode with a drop volume of 3 μL. The results correspond to the average of at least 3 measurements.

Time-of-Flight Secondary-Ion Mass Spectrometry (ToF-SIMS).
Time of Flight Secondary Ion Mass Spectrometry measurements of SAMs were carried out using a TOF-SIMS 5 time-of-flight secondary ion mass spectrometer (IONTOF GmbH), equipped with a liquid metal ion gun (LMIG) orientated at 45° to the sample surface. The LMIG provided a 10 micron-diameter 30 keV Bi_3^+ ion beam, operating at an ion current of 0.3 pA. Analyses were performed over an area of 500 × 500 μm^2. Flood gun (21V) was applied to SAMs deposited on silicon wafer to avoid charging effects.

X-ray photoelectron spectroscopy (XPS).
XPS analyses were performed using an Omicron Argus X-ray or a Thermo Fisher Alpha 110 photoelectron spectrometer, equipped with a monochromated AlKα radiation source (hν = 1486.6 eV), and a 150 W or a 300 W electron beam power respectively. The emission of photoelectrons from the sample was analyzed at a takeoff angle of 45° for Omicron Argus X-ray or 90° for Thermo Fisher Alpha 110 under ultra-high vacuum conditions ($\leq 10^{-9}$ mbar). Spectra were carried out with 100 eV pass energy for the survey scan and 20 eV pass energy for the C 1s, O 1s, and N 1s regions. Binding energies were calibrated against the C 1s (C–C) binding energy at 284.8 eV and element peak intensities were corrected by Scofield factors.[31] The peak areas were determined after subtraction of a Shirley background. The spectra were fitted using Casa XPS v.2.3.15 software (Casa Software Ltd, U.K.) and applying a Gaussian/Lorentzian ratio equal to 70/30.

SERS measurements.
SERS measurements were carried out in backscattering geometry under 633 nm laser irradiation (1 % density filter) using a LabRAM HR800 spectrometer equipped with a motorized xy stage, a 600 grooves/mm diffraction grating, and a short-working-distance ×100 Olympus objective with 0.90 numerical aperture. The integration time was 240 s per spectral window.
A video camera allowed for the visualization of samples prior to laser excitation. SERS measurements were performed on sample regions, which appeared yellowish on the video images, thus suggesting a high density of gold NRs.

Transmission electron microscopy (TEM).
TEM measurements were performed using a JEOL 1400 microscope that operates at 200 kV. The samples were prepared by depositing one drop of the colloidal dispersion on a conventional carbon-coated copper grid. The grids were then air-dried at room temperature and stored in a closed box to prevent dust accumulation.

Zeta potential measurements:
The ζ potential measurement was recorded on WALLIS^{TM} analyzer based on Laser Doppler Electrophoresis (LDE) measurement technology (Cordouan TechnologiesTM, Pessac, France). Before the measurement, GNRs were dispersed in a 1 mM HEPES buffer (pH=7.4) and placed in the dip cell composed of amorphous carbon electrodes. The measurement was repeated 6 times for each batch.

UV-visible absorption spectroscopy.
Absorption spectra were taken on AuNR dispersions diluted by a factor of 10 using a Shimadzu spectrophotometer in a 1 cm quartz cell.

3. Results and discussion

3.1 Deposition of organosilane bearing end-phthalimide group by spin coating: influence of temperature and time.

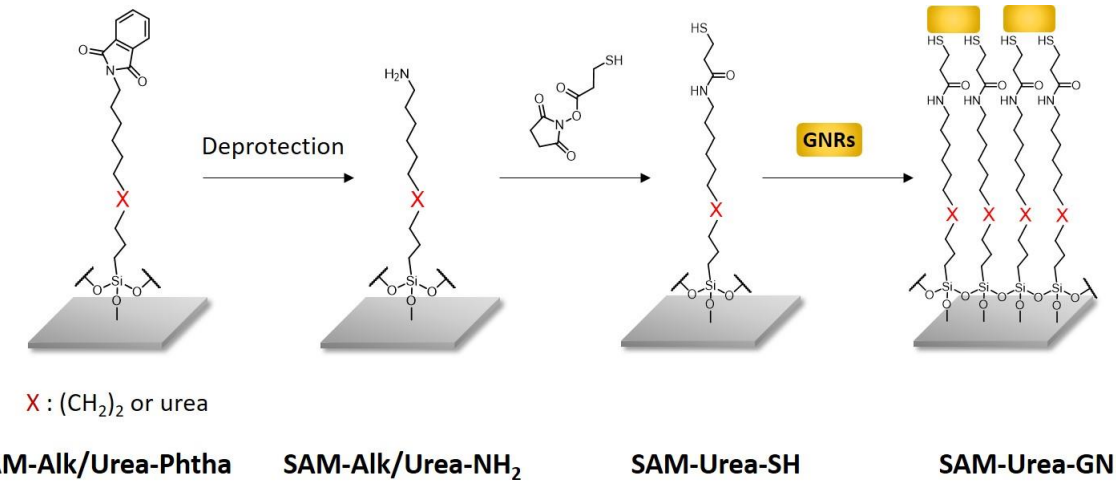

Scheme 1. Schematic representation of the preparation of SAMs-NH_2 and its reaction with bifunctional heterolinker MPH following by the immobilization of GNRs.

PM-IRRAS, wettability and AFM studies

For the preparation of well-defined amino-terminated SAMs, we used the N-phthalimide protected aminosilanes to avoid the multiple interaction of the amine end group with the polar groups available on the silica surface. Two phthalimide trimethoxy silanes bearing an alkyl chain or a urea group as a spacer were used to afford the corresponding **SAM-Alk-Phtha** and **SAM-Urea-Phtha**. These two SAMs were prepared by using the spin coating technique for the deposition of organosilanes followed by a drying step at ambient atmosphere to achieve hydrolysis-condensation reaction. Finally, a washing process in ultrasonic bath removed the excess of organosilanes. In a previous study, we described the preparation of these two SAMs at RT. For **SAM-Alk-Phtha** and **SAM-Urea-Phtha** the drying step duration were 14 hrs and 6 hrs long, respectively.[28] To shorten the drying step, the curing effect in air has been investigated for different times. The PM-IRRAS spectra of **SAM-Urea-Phtha** and **SAM-Alk-Phtha** are presented in Figures 1 and 2 in the 3100-1350 cm^{-1} spectral range for different curing conditions. **SAM-Urea-Phtha** was exposed to seven different curing conditions: curing for 10 min, 15 min, 30 min, 1 hr, 3 hrs and 6 hrs at 100 °C. The PM-IRRAS spectrum of the SAM produced at RT for 6 hrs was taken as a reference. For each curing condition, the characteristic vibrational bands of the urea compound were observed on the silica surface: the antisymmetric (ν_aCH_2) and symmetric (ν_sCH_2) stretching modes of methylene groups at 2927 and 2958 cm^{-1}, respectively, the in-plane ($\nu C{=}O_{ip}$) and out-of-plane ($\nu C{=}O_{op}$) stretching modes of the carbonyl groups of the phthalimide moiety at 1773 and 1715 cm^{-1}, respectively, and the amide I and amide II of the urea group at 1630 and 1571 cm^{-1}, respectively. For **SAM-Urea-Phtha**, the self-assembly of molecules is mainly controlled by intermolecular hydrogen bonding. The wavenumber difference ($\Delta\nu$) between amide I and amide II was used to verify the presence of hydrogen bonding. The $\Delta\nu$ values around 60 cm^{-1} confirm the strong association of urea group by hydrogen bonding.[28]

An estimation of the monolayer's thickness has been performed for **SAM-Urea-Phtha** by simulating the PM-IRRAS spectra at various thicknesses using the isotropic optical constants of **Urea-Phtha** compound. The optical constants (refractive index and extinction coefficient) of **Urea-Phtha** compound have been determined in the infrared spectral range from polarized attenuated total reflectance (ATR) spectra using a known procedure (Supporting information (SI), Figures S1a and S1b).[24,32] Using the linear dependence of the IRRAS intensity of the ν_aCH_2 mode with the monolayer thickness (SI, Figure S2), the IRRAS intensity of 0.00128 measured for the ν_aCH_2 mode of **SAM-Urea-Phtha** corresponds to a thickness of 15.3 Å for **SAM-Urea-Phtha**, which is in agreement with the thickness of a single monolayer. The overall intensities of the PM-IRRAS spectra obtained by annealing at 100 °C for more than one hour are significantly higher than those of the SAM prepared at RT, which reveals the presence of a larger quantity of material than expected for a single monolayer (Figure 1a). In contrast, for duration shorter than one hour at 100 °C, the intensities of IRRAS spectra are close to those measured for the monolayer at RT. On the basis of the intensities of the methylene and amide bands, heat treatments at 100 °C for less than 30 min seems to produce a monolayer similar to that obtained at RT. By setting a temperature of 100 °C for the drying step, the time is thus significantly reduced from 6 hrs to less than 30 min to have SAMs with similar quality. The slightly different relative intensities observed for the bands of phthalimide end groups can be explained by orientation effects.

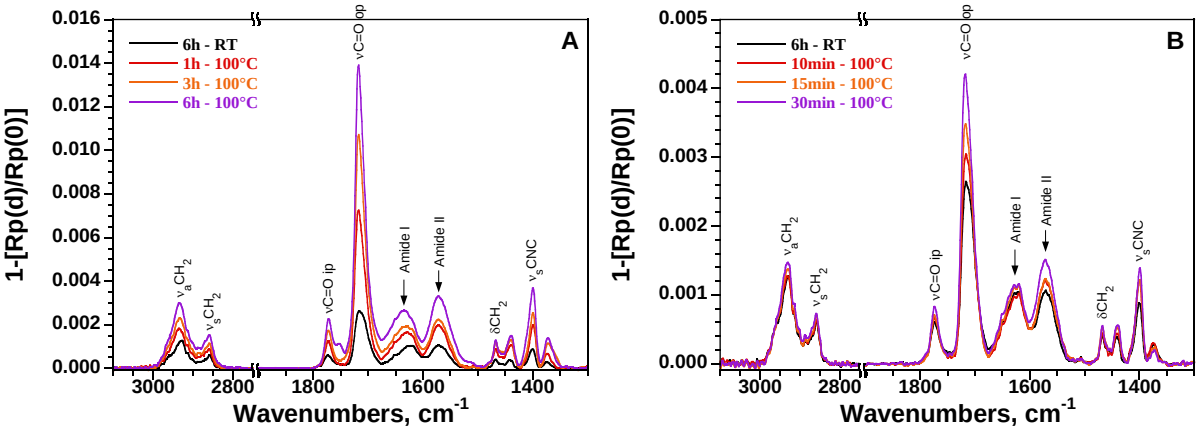

Figure 1. PM-IRRAS spectra of the **SAM-Urea-Phtha** depending on the curing conditions. **SAM-urea-Phtha** prepared at 100°C for (A) 1 hr, 3 hrs, 6 hrs and (B) for 10 min, 15 min, 30 min and SAM prepared at RT for 6 hrs was taken as a reference.

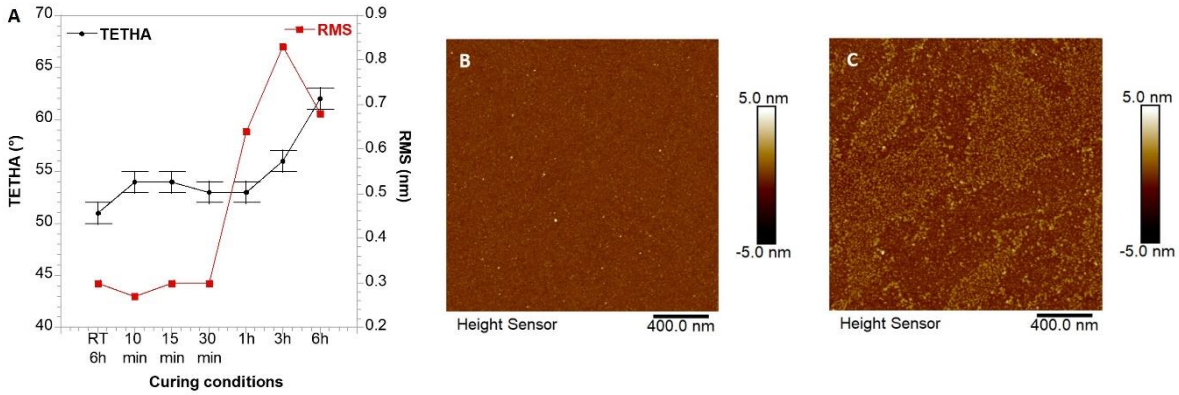

Figure 2. Water contact angle measurements and roughness for **SAM-urea-Phtha** prepared at RT for 6 hrs and 100°C for 10 min, 15 min, 30 min, 1 hr, 3 hrs and 6 hrs (A) and AFM height images (2 μm × 2 μm) of **SAM-Urea-Phtha** prepared with a drying step at 30 min (B) and 1 hr (C).

The water contact angle measurements and the root-mean-square (rms) roughness are consistent with the PM-IRRAS results (Figure 2). For drying times shorter than 1 hr at 100 °C, the contact angle values are close to 53° with rms roughness around 0.3 nm, which is similar to the values obtained for SAMs dried at RT for 6 hrs. For drying times longer than 1 hr at 100 °C, the contact angle value increases continuously and reaches 62° for a 6 hrs drying time. The increase in rms roughness is also significant, with values higher than 0.6 nm. The AFM height images for 1 hr, 3 hrs and 6 hrs are clearly not homogenous with a quantity of material exceeding the expected quantity for a monolayer, certainly due to the formation of aggregates. For 10 min, 15 min and 30 min, the AFM images are very homogeneous, as expected for a monolayer.

The PM-IRRAS spectra for **SAM-Alk-Phtha** prepared at 100 °C for the drying step are compared with the spectrum of the SAM prepared at RT corresponding to a monolayer (Figure 3). Indeed, the IRRAS intensity around 0.0020 for the $\nu_a CH_2$ mode of **SAM-Alk-Phtha** (14 hrs-RT) is consistent with the thickness of a single monolayer (13.0 Å) using the linear dependence of the IRRAS intensity of the $\nu_a CH_2$ mode with the monolayer thickness reported in SI (Figure S4). For all curing conditions, the characteristic vibrational bands of the corresponding organosilane were observed. The overall intensities of spectra for 10 to 30 min curing are lower than the intensity of the reference spectrum at RT. For **SAM-Alk-Phtha** heated 1 hr at 100 °C, the PM-IRRAS spectrum is similar to the one measured for the SAM left at RT. These results are consistent with the water contact angle values increasing up to 60° for a 1 hr long drying time, which is very close to the value measured for the monolayer at RT (Figure 4). The rms roughness measurements of all **SAM-Alk-Phtha** with curing at 100 °C were lower than 0.5 nm and AFM height images were homogeneous. Based on PM-IRRAS, wettability and AFM analysis, a drying step at 100 °C for 1 hr is optimum to have a homogeneous monolayer **SAM-Alk-Phtha**. Interestingly, hydrogen-bound SAMs require half drying time compared to SAMs based on van-der-Waals interactions. The hydrolysis condensation rate faster for ureido silane than for alkyl silane has already been observed for monolayers produced by immersion solution method.[12,33] Hydrogen-bonding interaction enables faster self-organization, which accelerates the polymerization reaction. This result highlights the advantage of self-assembly directed by intermolecular hydrogen bonding for fast preparation of SAMs.

ToF-SIMS investigation

ToF-SIMS measurements were carried out on **SAM-Alk-Phtha** (1 hr at 100 °C) and **SAM-Urea-Phtha** (30 min at 100 °C) on silicon wafer in positive and negative mode (see data in SI). For **SAM-Alk-Phtha** and **SAM-Urea-Phtha**, three characteristic ion fragments were assigned to the phthalimide terminal group in positive mode at m/z 130 ($C_8H_4NO^+$), 160 ($C_9H_6NO_2^+$) and in negative mode at m/z 146 ($C_8H_4NO_2^-$). These peaks are not observed on the positive and negative modes of ToF-SIMS spectra of silicon wafer without SAMs. In negative mode, m/z 26 (CN^-) and 42 (CNO^-) are also common fragments which characterize the presence of nitrogen atom in the organosilanes.[34] Interestingly, in positive mode, m/z 30 (CH_4N^+) was assigned to the urea group because this peak was observed only for **SAM-Urea-Phtha**. For **SAM-Alk-Phtha** and **SAM-Urea-Phtha,** m/z 77 ($C_6H_5^+$) corresponds to the alkyl chain. ToF-SIMS analysis clearly shows the characteristic molecular signature of the two organosilanes onto the surface. The mapping images of secondary ion fragment m/z 146 ($C_8H_4NO_2^-$) for **SAM-Alk-Phtha** and **SAM-Urea-Phtha** were homogeneous, which shows the ability of spin coating to cover the surface homogeneously at the micron scale.

However, for both SAMs, entire molecular ions were never detected. The hypothesis is that the molecules are strongly anchored to the surface due to their polymerization.[35]

ToF-SIMS analyses were carried out on organosilanes films freshly deposited by spin coating without drying step. For organosilane films with **Alk-Phtha** and **Urea-Phtha**, three ion fragments typical of the alkoxysilyl group are identified in positive mode at m/z 59 ($SiOCH_3^+$), 91 ($HSi(OCH_3)_2^+$) and 121 ($Si(OCH_3)_3^+$). The presence of these ions confirms that organosilanes were weakly hydrolyzed immediately after deposition on the substrate. These ion fragments are never detected on the monolayers showing a complete hydrolysis-condensation reaction of the organosilanes. In both organosilane films, the molecular ions fragments were detected in positive and negative modes, which is consistent with weak attachment of organosilanes on the surface due to the incomplete polymerization. These observations clearly show that the organosilanes are strongly anchored to the substrate by polymerization.

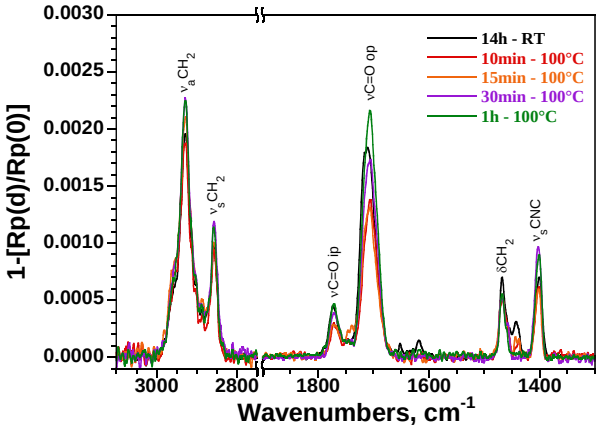

Figure 3. PM-IRRAS spectra of the **SAM-Alk-Phtha** for several curing conditions.

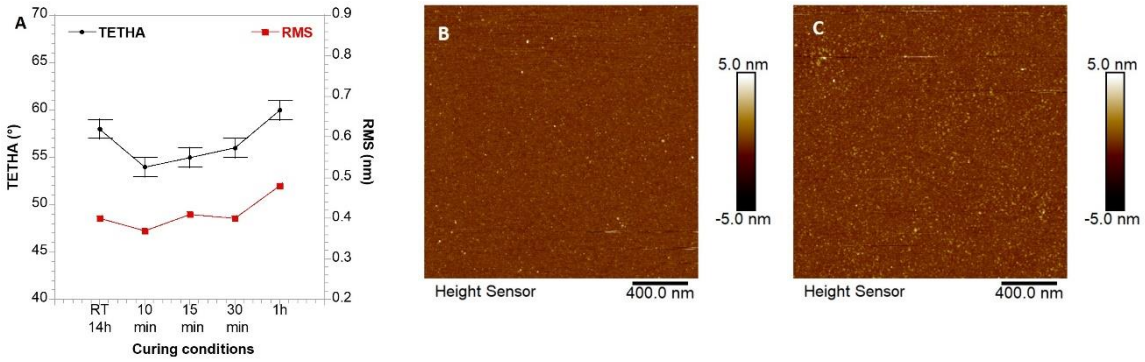

Figure 4. Water contact angle measurements and rms roughness for **SAM-Alk-Phtha** prepared at RT for 14 hrs and at 100 °C for 10 min, 15 min, 30 min and 1 hr (A) and AFM height images (2 μm × 2 μm) of **SAM-Alk-Phtha** prepared with a drying step at RT for 14 hrs (B) and 1 hr (C).

X-ray photoelectron spectroscopy measurements

SAM-Alk-Phtha (14 hrs at RT) and **SAM-Urea-Phtha** (30 min at 100 °C) on silicon wafer were investigated by XPS. Survey spectra as well as high resolution spectra were recorded at the C1s, O1s, N1s and Si2p edges.

First of all, one can notice the appearance of nitrogen in the elemental composition (Table 1 and survey spectra in Figure S9) together with a decrease of the silicon signal due to the presence of an organic layer. This clearly confirmed the presence of the SAM on the silica surfaces, as already confirmed by PM-IRRAS experiments.

Secondly, the elemental composition was assessed for both SAMs and is presented in Table 1, showing expected differences between the systems. Indeed, **SAM-Urea-Phtha** bearing urea group CO(**NH**)CO exhibits 5 times more nitrogen atoms than alkyl SAMs bearing only one nitrogen atom due to the phthalimide moiety.

Table 1. Elemental composition (atomic %) determined by XPS for both alkyl and urea **SAM-Phtha**.

	C1s	O1s	N1s	Si2p	N/C_{exp}	N/C_{th}
Si wafer	14.1	36.3	0.4	49.2	--	--
SAM-Alk-Phtha	24.1	33.8	1.1	41.0	0.046	0.061
SAM-urea-Phtha	31.4	26.1	5.5	36.9	0.175	0.19

In addition, in order to prove the integrity of the linker, the ratio C/N can be calculated and compared to the theoretical one. For **SAM-Alk/Urea-Phtha,** experimental ratios are slightly lower than theoretical ones due to the overestimation of the C1s atomic percentage (carbonaceous contamination and small deposition of carbon by the XPS source, always observed on organic layer deposited from solution on surfaces and also observed on the bare Si wafer). However, the experimental values of these ratios also prove the integrity of the adsorbed molecule.

As mentioned above, the photoelectron signal of a substrate covered by an organic layer decreases with respect to a pristine substrate due to its attenuation when crossing the layer. As XPS is quantitative, it allows the thickness of the organic layer to be estimated by measuring the decrease of the substrate photoelectron signal using a mathematical model.

In our case, the silicon wafer first exhibits the formation of native SiO_2 oxide on its subsurface, as corroborated by the presence of O1s (Table 1). On XPS spectra, the native SiO_2 oxide appears at higher binding energy than pristine silicon (Figure 5, blue spectrum). The photoelectron signal assigned to the adsorbed silane moiety shows the same binding energy as SiO_2, thus a different one from Si (Figure 5, red spectrum). Consequently, the subtraction of the SiO_2 signal from the sum signal including SiO_2 and Si-O-Silane contributions lead to the contribution of the adsorbed silane alone, which can then be used to estimate the thickness of the organic layer.

Using equation 1, the equivalent thicknesses of the two SAMs were calculated to be 15.5 Å for the **SAM-urea-Phtha** and 11.1 Å for the **SAM-Alk-Phtha**. These calculated thicknesses are lower than the theoretical length of the two organosilanes with an *all*-trans conformation of the alkyl chains which are approximately 20Å and 19Å, respectively for compounds **1** (**Si-Urea-Phtha)** and **2 (Si-Alk-Phtha)**. Depending on the orientation of the molecule, the thickness should be equal to or less than the molecular length in linear conformation. These two equivalent thicknesses calculated in XPS are in good agreement with that of a monolayer adsorbed on silica surface. In addition, these results are consistent with the disordered alkyl chain observed in PM-IRRAS which confirms the formation of a monolayer by using the spin coating technique. Thus, these results also showed that a monolayer was obtained whatever the drying step conditions (RT or 100°C).

$$d = \lambda_{Si2p}^{SiO_2} \cos\theta \,.\, ln\left(1 + \frac{I_{SiO_2}.M_{SiO_2}.\rho_{Si}.\lambda_{Si2p}^{Si}}{I_{Si}.M_{Si}.\rho_{SiO_2}.\lambda_{Si2p}^{SiO_2}}\right)$$ (eq 1, adapted from [36])

where d is the equivalent thickness, λ_x^y is the mean free path of photoelectron *x* in a *y* matrix, I_x, M_x en ρ_x are respectively the intensity, the molecular weight, and the density of element *x*, and θ is the collection angle of photoelectrons.

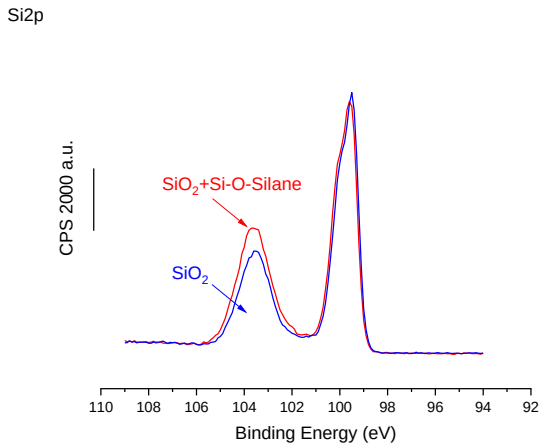

Figure 5. XPS Si2p high-resolution region for **SAM-Alk-Phtha** (red trace) compared to the bare silicon wafer (blue trace), CPS = Count Per Second.

3.2 Removal of protecting group and derivatization with MPH

SAM-Alk-Phtha and **SAM-Urea-Phtha** prepared using the best heat treatment conditions (ca 1 hr and 30 min at 100 °C, respectively) were converted into amino-terminated SAMs. SAM-Phtha were immersed in an aqueous solution of methylamine for several minutes to afford the corresponding **SAM-Alk/Urea-NH2**.[37] PM-IRRAS spectra before and after deprotection are presented in Figure 6a and 6b and confirm the successful reaction by the disappearance of the two characteristic bands of the phthalimide moiety at 1773 cm^{-1} ($\nu C{=}O_{ip}$) and 1715 cm^{-1} ($\nu C{=}O_{op}$). A new broad band appeared at around 1645 cm^{-1} assigned to the bending mode (δNH_2) of the amino groups. After deprotection, monolayers became more hydrophilic with contact angles of 42° ± 1 and 45° ± 1 for **SAM-Urea-NH2** and **SAM-Alk-NH2**, respectively.

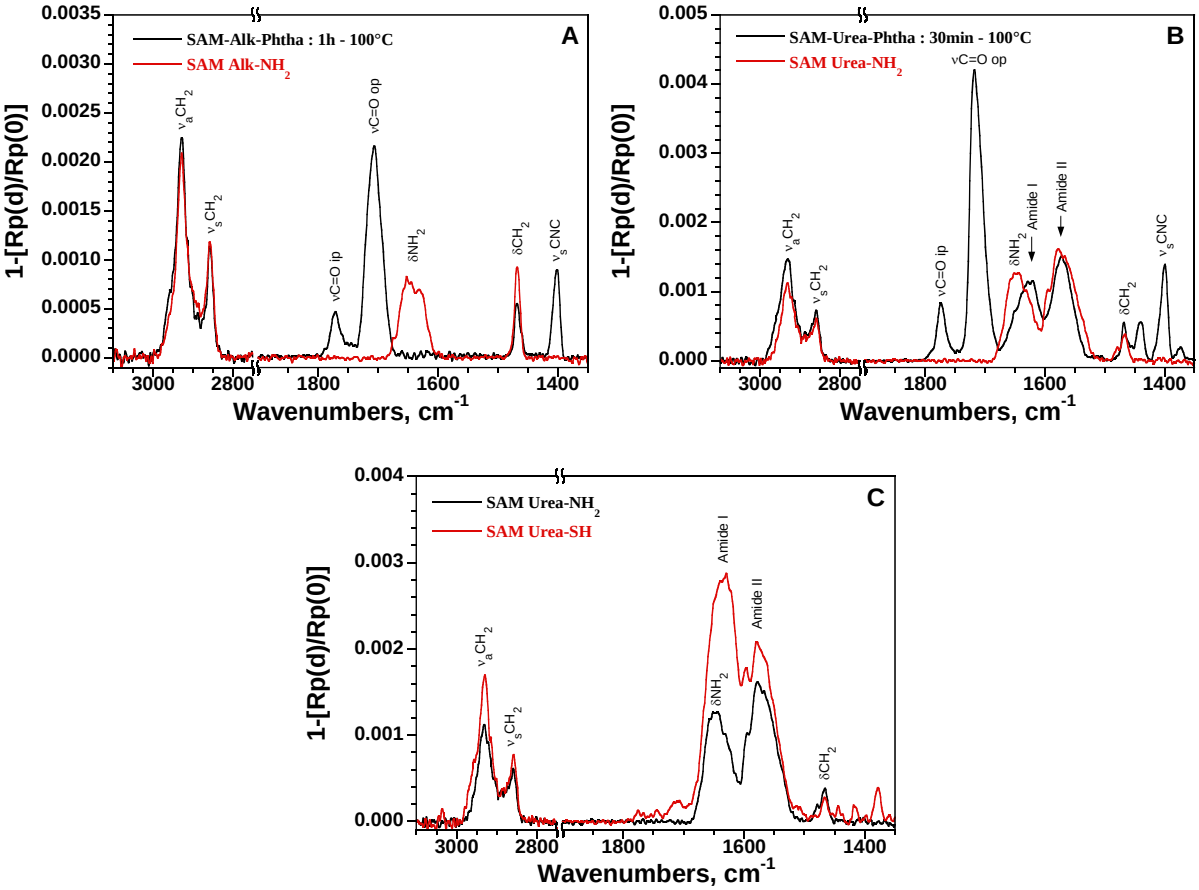

Figure 6. PM-IRRAS spectra of **SAM-Alk-Phtha** (A) and **SAM-Urea-Phtha** (B) before and after deprotection and the derivatization of **SAM-Urea-NH2** by MPH to afford **SAM-Urea-SH** (C).

ToF-SIMS measurements (see data in SI) were performed on **SAM-Alkyl/Urea-NH2**. The characteristic peaks of phthalimide group in positive and in negative modes at m/z 160 and m/z 146, respectively, disappeared, which is consistent with the PM-IRRAS observations showing a complete successful deprotection reaction.

XPS experiments were also performed on **SAM-Urea-NH2** to confirm the deprotection reaction of phtalimide into primary amine. Figure 7 presents the XPS spectra of N1s region before (bottom) and after (top) the deprotection of **SAM-Urea-Phtha.** On the spectrum of **SAM-Urea-Phtha**, two contributions were clearly observed at binding energy of 399.0 eV and 400.0 eV,

assigned respectively to N atoms in phthalimide groups and to N atoms in -NH- urea environment,[38] with a ratio of 0.5 as expected from the formula (1:2) of the molecule in Figure 7. After deprotection, the spectrum associated with **SAM-Urea-NH$_2$** changes drastically from the previous one. No low binding energy contribution could be seen at 399.0 eV, and the main contribution assigned to urea (-NH-) and terminal amino groups is centered at 400.0 eV. In addition, the weak contribution discerned at higher binding energy, i.e. 402.0 eV, is usually assigned to protonated amino groups (NH_3^+).[39] This contribution is much lower than the main one, suggesting that both neutral and zwitterionic forms of free amine co-exist in the SAMs with a ratio NH_2:NH_3^+ estimated at 2:1 from integrated area under peak in the XPS spectrum of Figure 7. The presence of NH_3^+ can be explained by the protonation of NH_2 by ambient moisture.[13] A higher proportion of NH_2 group could be obtained by deprotection in a basic solution.[40]

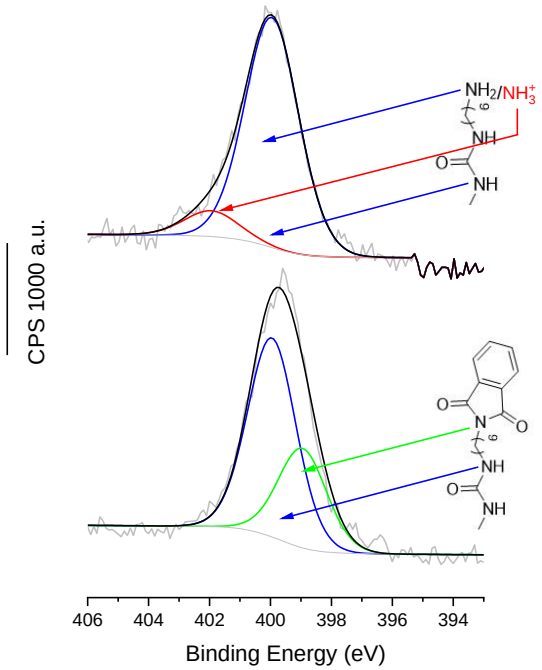

Figure 7. XPS High-resolution spectra of the N1s region before (bottom: **SAM-Urea-Phtha**) and after (top: **SAM-Urea-NH$_2$**) phthalimide deprotection, CPS = Count Per Second.

Thiol-terminated SAMs were prepared from **SAM-Urea-NH$_2$** after reaction with the cross-linker MPH. The coupling reaction was performed between the amino end group of the monolayer and the succinimidyl ester group of MPH to afford the amide bond. The PM-IRRAS spectra of **SAM-Urea-NH$_2$** and **SAM-Urea-SH** are compared in Figure 6c. For **SAM-Urea-SH** the intensities of methylene as well as amide I and amide II bands increased, which confirm the coupling reaction with the cross-linker MPH. The νSH band, expected around 2590 cm^{-1}, is too weak to be detected by PM-IRRAS. The presence of the thiol terminal group can be observed by negative mode ToF-SIMS analysis in Figure 8. For **SAM-Urea-SH**, ion fragments

m/z 31.972 (S^-) and 63.965 (SO_2^-) assigned to the thiol group were detected. These ions are not observed on **SAM-Urea-NH2,** which confirms the successful derivatization with MPH. The mapping images of secondary ions S^- and SO_2^- for **SAM-Urea-SH** are homogeneous showing the good reactivity of amino end groups of **SAM-Urea-NH2** with MPH at the micron-scale. **SAM-Urea-SH** is more hydrophobic than the initial **SAM-Urea-NH2** with contact angles of 52° ± 2° and 42° ± 1° respectively.

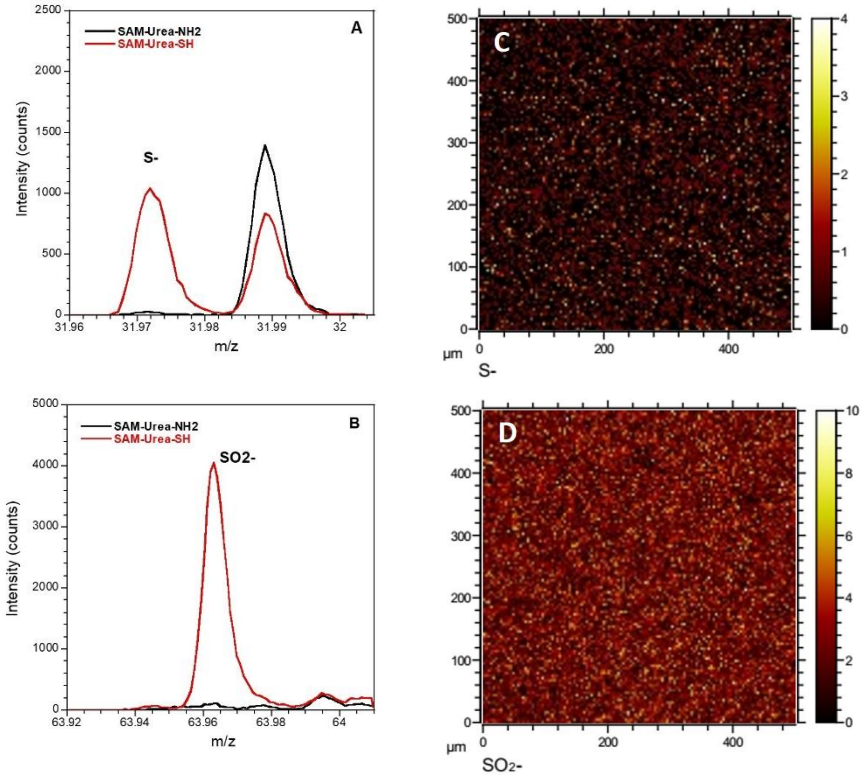

Figure 8. Negative mode ToF-SIMS spectra of secondary ions fragments m/z (A) 31.972 (S^-) and (B) 63.965 (SO_2^-) for **SAM-Urea-SH** and **SAM-Urea-NH2**, and mapping images (500 µm × 500 µm) of ions fragments (C) S^- and (D) SO_2^- for **SAM-Urea-SH.**

3.3 Immobilization of GNRs on thiol-terminated SAMs

SAMs can be used to immobilize gold nanoparticles yielding powerful SERS substrates.[41,42] The immobilization of pre-synthesized GNRs were performed on homogeneous **SAM-Urea-SH** to afford **SAM-Urea-GNRs.** GNRs were synthesized by a seedless colloidal approach. This single-step approach yielded CTAB-coated particles with an aspect ratio of 2.9 and a yield as high as 95% (Figures S6 and S7). To facilitate GNRs grafting onto **SAM-Urea-SH**, the CTAB surfactant bilayer adsorbed on the nanoparticles surface was displaced by PVP macromolecules according to the process detailed in the experimental section. As the interactions between particle and polymer are weak (Van der Waals forces), this allows the particles to be rapidly immobilized during the deposition step.[43] CTAB-coated GNRs displayed a zeta potential of approximately +40 ± 5 mV at pH 7.4 while the zeta potential of GNRs decreased to a value of +11.8 ± 1.6 mV after ligand exchange with PVP. This decrease means either that the PVP macromolecular layer pushes the slip plane away from the GNR surface or that the outer layer

loses positive charges upon ligand exchange. After CTAB displacement, no significant shift or broadening of LSPR bands was observed (Figures S7 and S8). The TEM image confirms the preservation of particle shape and size after surface modification. **SAM-Urea-SH** was then incubated in a dispersion of PVP-stabilized GNRs. After the washing process in an ultrasonic bath with different solvents (Milli-Q water, ethanol and chloroform) the resulting modified surface was examined by AFM. AFM images (Figure 9a and 9b) confirm the presence of individualized and closely contacted nanorods on the **SAM-Urea-SH** with a homogeneous distribution even after the successive washing steps. Gold surfaces are well-known to form strong and stable bond to molecules with thiols (Au-S ~50 Kcal.mol^{-1}). **SAM-Urea-NH$_2$** was also incubated with the similar solution of GNRs to evaluate the non-specific adhesion. AFM images (Figure 9c) clearly show the absence of nanorods on **SAM-Urea-NH$_2$**. This result indicates that the attachment of GNRs onto **SAM-Urea-SH** is performed through Au-S bonding between the thiolated SAM and the GNRs. These two-dimensional nanorod monolayer is potentially interesting as SERS platform for the detection of biomolecules.[44] To assess the existence of possible SERS active sites on **SAM-Urea-NRs**, an oligonucleotide with a terminal thiol at the 5' position was grafted on immobilized GNRs. SERS spectra were measured before and after the grafting of the oligonucleotide on **SAM-Urea-NRs** (Figure 10). The two SERS spectra exhibit an intense background which could be associated with inelastic light scattering from the SAM-substrate system. The maximum of this background has been shown to coincide with the localized surface plasmon resonance (LSPR) of excited metal nanoparticles.[45,46] In our case, the maximum of the background is centered at nearly 1100 cm^{-1} under 633 nm irradiation, which corresponds to a LSPR centered at $\lambda_{LSPR}=\lambda_{max}=$ 680 nm, in good agreement with expectations for gold NRs with 2.9 aspect ratio.[47] Moreover, additional SERS bands are observed in the presence of the oligonucleotide. In the two SERS spectra, Raman bands assigned to CH stretching vibrations of alkyl chains of **SAM-Urea-NRs** in the 2830-3000 cm^{-1} spectral range are visible. However, a more intense contribution is observed at 2862 cm^{-1}, when the oligonucleotide is added to the sample. More interestingly, vibration modes that are specific to DNA nucleobases, such as the ring breathing modes of adenine at 733 cm^{-1} and guanine at 682 cm^{-1}, and to the DNA backbone, such as the vibration mode of ribose-phosphate at 956 cm^{-1}, can be discerned.[48,49] This confirms the ability to identify oligonucleotides using **SAM-Urea-NRs**.

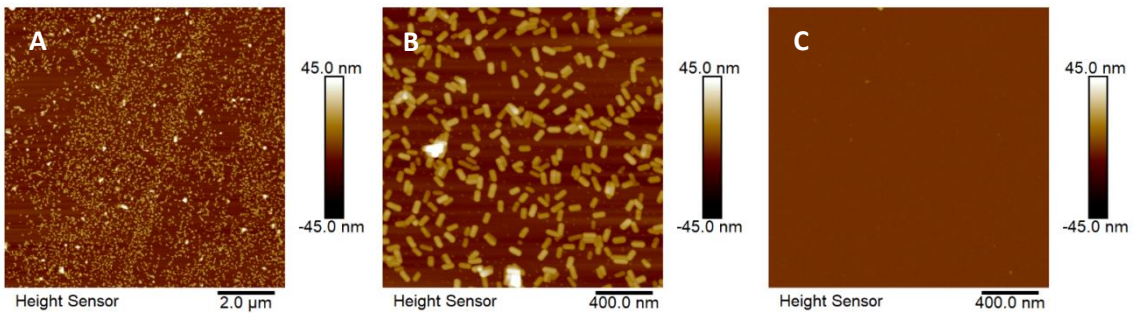

Figure 9. AFM height images of **SAM-Urea-NRs** (A: 10 µm × 10 µm, B: 2 µm × 2 µm), and **SAM-Urea-NH$_2$** after tentative immobilization of GNRs (C: 2 µm × 2 µm).

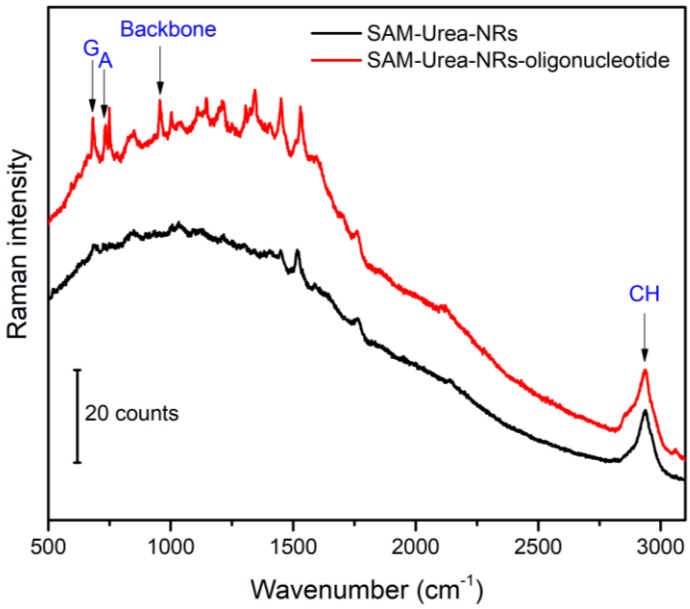

Figure 10. SERS spectra of **SAM-Urea-GNRs** without and with DNA-strand. The normalization has been performed by equaling intensities of Raman bands at 2935 cm^{-1}.

4. Conclusion

In this work, the optimization of a monolayer deposition by spin coating was studied. We shown that the drying step is essential for the hydrolysis condensation reaction to obtain robust monolayers. Following an accurate optimization methodology, we were able to significantly reduce the drying time. For **SAM-Alk-Phtha** and **SAM-Urea-Phtha,** the drying times at 100°C were 1 hr and 30 min respectively, instead of 14 hrs and 6 hrs at RT.[28] SAMs performed at RT or 100°C have equivalent qualities in term of wettability and topography. The spin coating technique combined with the annealing step thus appears as an excellent way for rapid and easy functionalization of planar substrates with SAMs in ambient conditions and using only few organic solvent.

In addition, PM-IRRAS and XPS measurements clearly showed that SAMs prepared by the spin coating with drying step at RT or 100°C consisted in a single monolayer. ToF-SIMS analysis also showed the strong anchoring of organosilanes by polymerization in the two monolayers. The kinetics of the polymerization reaction depend on the molecular structure of the organosilanes. The self-assembly of ureido-silanes by intermolecular hydrogen bonding halves the drying time compared with alkyl-silanes. **SAM-Phtha** were easily deprotected within minutes to give amino-terminated SAMs. From **SAM-Urea-NH_2**, a thiol-terminated-SAM was obtained and has demonstrated its ability to strongly immobilize PVP-coated GNRs with a homogenous distribution over the substrate. The resulting molecular platform decorated with gold nanorods showed SERS activity, as exemplified by the detection of an oligonucleotide. In addition, the strong anchoring of the GNRs on SAMs opens the way to reuse of these SERS active substrates and possible regeneration as biosensors. Even though improvements are still needed (limits of detection, readout time, sample volume…), this proof-of-concept study demonstrates the relevance of the developed silane-based method to design SERS platforms for biosensing.

Acknowledgements

The authors gratefully acknowledge financial supports from Bordeaux University and the National Center for Scientific Research (CNRS). PM-IRRAS and SERS measurements were performed at the platform SIV (Spectroscopie et Imagerie Vibrationnelle) funded by the European Union (FEDER), the Région Nouvelle Aquitaine and the University of Bordeaux. This work was partly supported by the French RENATECH network and its FEMTO-ST technological facility for Alpha 110 XPS analysis. The authors also acknowledge IMPC from Sorbonne University (Institut des Matériaux de Paris Centre, FR CNRS 2482) and the C'Nano projects of the Region Ile-de-France, for Omicron XPS apparatus funding. This work has been partially supported by Labex ARCANE and CBH-EUR-GS (ANR-17-EURE-0003).

References

(1) Choi, Y.; Tran, H.-V.; Lee, T. R. Self-Assembled Monolayer Coatings on Gold and Silica Surfaces for Antifouling Applications: A Review. *Coatings* **2022**, *12* (10), 1462. https://doi.org/10.3390/coatings12101462.

(2) Watson, S.; Nie, M.; Wang, L.; Stokes, K. Challenges and Developments of Self-Assembled Monolayers and Polymer Brushes as a Green Lubrication Solution for Tribological Applications. *RSC Adv.* **2015**, *5* (109), 89698–89730. https://doi.org/10.1039/C5RA17468F.

(3) Yi, R.; Mao, Y.; Shen, Y.; Chen, L. Self-Assembled Monolayers for Batteries. *J. Am. Chem. Soc.* **2021**, *143* (33), 12897–12912. https://doi.org/10.1021/jacs.1c04416.

(4) Singh, M.; Kaur, N.; Comini, E. The Role of Self-Assembled Monolayers in Electronic Devices. *J. Mater. Chem. C* **2020**, *8* (12), 3938–3955. https://doi.org/10.1039/D0TC00388C.

(5) Oliverio, M.; Perotto, S.; Messina, G. C.; Lovato, L.; De Angelis, F. Chemical Functionalization of Plasmonic Surface Biosensors: A Tutorial Review on Issues, Strategies, and Costs. *ACS Appl. Mater. Interfaces* **2017**, *9* (35), 29394–29411. https://doi.org/10.1021/acsami.7b01583.

(6) Vashist, S. K.; Lam, E.; Hrapovic, S.; Male, K. B.; Luong, J. H. T. Immobilization of Antibodies and Enzymes on 3-Aminopropyltriethoxysilane-Functionalized Bioanalytical Platforms for Biosensors and Diagnostics. *Chem. Rev.* **2014**, *114* (21), 11083–11130. https://doi.org/10.1021/cr5000943.

(7) Iorio, D. D.; Huskens, J. Surface Modification with Control over Ligand Density for the Study of Multivalent Biological Systems. *ChemistryOpen* **2020**, *9* (1), 53–66. https://doi.org/10.1002/open.201900290.

(8) Pujari, S. P.; Scheres, L.; Marcelis, A. T. M.; Zuilhof, H. Covalent Surface Modification of Oxide Surfaces. *Angewandte Chemie International Edition* **2014**, *53* (25), 6322–6356. https://doi.org/10.1002/anie.201306709.

(9) Li, N.; Li, T.; Qiao, X.-Y.; Li, R.; Yao, Y.; Gong, Y.-K. Universal Strategy for Efficient Fabrication of Blood Compatible Surfaces via Polydopamine-Assisted Surface-Initiated Activators Regenerated by Electron Transfer Atom-Transfer Radical Polymerization of Zwitterions. *ACS Appl. Mater. Interfaces* **2020**, *12* (10), 12337–12344. https://doi.org/10.1021/acsami.9b22574.

(10) Meillan, M.; Ramin, M. A.; Buffeteau, T.; Marsaudon, S.; Odorico, M.; Chen, S. W.; Pellequer, J.-L.; Degueil, M.; Heuzé, K.; Vellutini, L.; Bennetau, B. Self-Assembled Monolayer for AFM Measurements of Tobacco Mosaic Virus (TMV) at the Atomic Level. *RSC Adv.* **2014**, *4* (23), 11927–11930. https://doi.org/10.1039/C3RA46716C.

(11) Wasserman, S. R.; Tao, Y. T.; Whitesides, G. M. Structure and Reactivity of Alkylsiloxane Monolayers Formed by Reaction of Alkyltrichlorosilanes on Silicon Substrates. *Langmuir* **1989**, *5* (4), 1074–1087. https://doi.org/10.1021/la00088a035.

(12) Ramin, M. A.; Le Bourdon, G.; Heuzé, K.; Degueil, M.; Belin, C.; Buffeteau, T.; Bennetau, B.; Vellutini, L. Functionalized Hydrogen-Bonding Self-Assembled Monolayers Grafted onto SiO2 Substrates. *Langmuir* **2012**, *28* (51), 17672–17680. https://doi.org/10.1021/la303805d.

(13) Ding, L.; Fang, Y.; Blanchard, G. J. Probing the Effects of Cholesterol on Pyrene-Functionalized Interfacial Adlayers. *Langmuir* **2007**, *23* (22), 11042–11050. https://doi.org/10.1021/la701310f.

(14) Ramin, M. A.; Le Bourdon, G.; Heuzé, K.; Degueil, M.; Buffeteau, T.; Bennetau, B.; Vellutini, L. Epoxy-Terminated Self-Assembled Monolayers Containing Internal Urea or Amide Groups. *Langmuir* **2015**, *31* (9), 2783–2789. https://doi.org/10.1021/la5049375.

(15) Azam, Md. S.; Fenwick, S. L.; Gibbs-Davis, J. M. Orthogonally Reactive SAMs as a General Platform for Bifunctional Silica Surfaces. *Langmuir* **2011**, *27* (2), 741–750. https://doi.org/10.1021/la1041647.

(16) Al-Hajj, N.; Mousli, Y.; Miche, A.; Humblot, V.; Hunel, J.; Heuzé, K.; Buffeteau, T.; Genin, E.; Vellutini, L. Influence of the Grafting Process on the Orientation and the Reactivity of Azide-Terminated Monolayers onto Silica Surface. *Applied Surface Science* **2020**, *527*, 146778. https://doi.org/10.1016/j.apsusc.2020.146778.

(17) Wang, L.; Schubert, U. S.; Hoeppener, S. Surface Chemical Reactions on Self-Assembled Silane Based Monolayers. *Chem. Soc. Rev.* **2021**, *50* (11), 6507–6540. https://doi.org/10.1039/D0CS01220C.

(18) Aissaoui, N.; Bergaoui, L.; Landoulsi, J.; Lambert, J.-F.; Boujday, S. Silane Layers on Silicon Surfaces: Mechanism of Interaction, Stability, and Influence on Protein Adsorption. *Langmuir* **2012**, *28* (1), 656–665. https://doi.org/10.1021/la2036778.

(19) Dekeyser, C. M.; Buron, C. C.; Mc Evoy, K.; Dupont-Gillain, C. C.; Marchand-Brynaert, J.; Jonas, A. M.; Rouxhet, P. G. Oligo(Ethylene Glycol) Monolayers by Silanization of Silicon Wafers: Real Nature and Stability. *Journal of Colloid and Interface Science* **2008**, *324* (1), 118–126. https://doi.org/10.1016/j.jcis.2008.05.002.

(20) Millot, Y.; Hervier, A.; Ayari, J.; Hmili, N.; Blanchard, J.; Boujday, S. Revisiting Alkoxysilane Assembly on Silica Surfaces: Grafting versus Homo-Condensation in Solution. *J. Am. Chem. Soc.* **2023**, *145* (12), 6671–6681. https://doi.org/10.1021/jacs.2c11390.

(21) Kosovari, M.; Buffeteau, T.; Thomas, L.; Guay Bégin, A.-A.; Vellutini, L.; McGettrick, J. D.; Laroche, G.; Durrieu, M.-C. Silanization Strategies for Tailoring Peptide Functionalization on Silicon Surfaces: Implications for Enhancing Stem Cell Adhesion. *ACS Appl. Mater. Interfaces* **2024**, *16* (23), 29770–29782. https://doi.org/10.1021/acsami.4c03727.

(22) Heid, S.; Effenberger, F.; Bierbaum, K.; Grunze, M. Self-Assembled Mono- and Multilayers of Terminally Functionalized Organosilyl Compounds on Silicon Substrates. *Langmuir* **1996**, *12* (8), 2118–2120. https://doi.org/10.1021/la9504164.

(23) Martin, P.; Marsaudon, S.; Thomas, L.; Desbat, B.; Aimé, J.-P.; Bennetau, B. Liquid Mechanical Behavior of Mixed Monolayers of Amino and Alkyl Silanes by Atomic Force Microscopy. *Langmuir* **2005**, *21* (15), 6934–6943. https://doi.org/10.1021/la050288b.

(24) Siurdyban, E.; Brotin, T.; Heuzé, K.; Vellutini, L.; Buffeteau, T. Immobilization of Cryptophane Derivatives onto SiO_2 /Au and Au Substrates. *Langmuir* **2014**, *30* (49), 14859–14867. https://doi.org/10.1021/la5039156.

(25) Rouvière, L.; Al-Hajj, N.; Hunel, J.; Aupetit, C.; Buffeteau, T.; Vellutini, L.; Genin, E. Silane-Based SAMs Deposited by Spin Coating as a Versatile Alternative Process to Solution Immersion. *Langmuir* **2022**, *38* (20), 6464–6471. https://doi.org/10.1021/acs.langmuir.2c00668.

(26) Xiao, Z.; Cai, C.; Mayeux, A.; Milenkovic, A. The First Organosiloxane Thin Films Derived from $SiCl_3$ -Terminated Dendrons. Thickness-Dependent Nano- and Mesoscopic Structures of the Films Deposited on Mica by Spin-Coating. *Langmuir* **2002**, *18* (20), 7728–7739. https://doi.org/10.1021/la026001h.

(27) Sun, Y.; Negreira, A. R.; Meersschaut, J.; Hoflijk, I.; Vaesen, I.; Conard, T.; Struyf, H.; Tokei, Z.; Boemmels, J.; Moinpour, M.; De Feyter, S.; Armini, S. Optimization and Upscaling of Spin Coating with Organosilane Monolayers for Low-k Pore Sealing. *Microelectronic Engineering* **2017**, *167*, 32–36. https://doi.org/10.1016/j.mee.2016.10.011.

(28) Rouvière, L.; Hachin, A.; Shinkaruk, S.; Hunel, J.; Aupetit, C.; Buffeteau, T.; Genin, E.; Vellutini, L. Self-Assembly of Amino-Terminated Monolayers Depending on the Chemical Structure. *New J. Chem.* **2023**, *47* (20), 9661–9668. https://doi.org/10.1039/D3NJ01312J.

(29) Roach, L.; Ye, S.; Moorcroft, S. C. T.; Critchley, K.; Coletta, P. L.; Evans, S. D. Morphological Control of Seedlessly-Synthesized Gold Nanorods Using Binary Surfactants. *Nanotechnology* **2018**, *29* (13), 135601. https://doi.org/10.1088/1361-6528/aaa99d.

(30) Ramin, M. A.; Le Bourdon, G.; Daugey, N.; Bennetau, B.; Vellutini, L.; Buffeteau, T. PM-IRRAS Investigation of Self-Assembled Monolayers Grafted onto SiO2/Au Substrates. *Langmuir* **2011**, *27* (10), 6076–6084. https://doi.org/10.1021/la2006293.

(31) Scofield, J. H. Hartree-Slater Subshell Photoionization Cross-Sections at 1254 and 1487 eV. *Journal of Electron Spectroscopy and Related Phenomena* **1976**, *8* (2), 129–137. https://doi.org/10.1016/0368-2048(76)80015-1.

(32) Dignam, M. J.; Mamiche-Afara, S. Determination of the Spectra of the Optical Constants of Bulk Phases via Fourier Transform ATR. *Spectrochimica Acta Part A: Molecular Spectroscopy* **1988**, *44* (12), 1435–1442. https://doi.org/10.1016/0584-8539(88)80195-8.

(33) Dinh, D. H.; Vellutini, L.; Bennetau, B.; Dejous, C.; Rebière, D.; Pascal, E.; Moynet, D.; Belin, C.; Desbat, B.; Labrugère, C.; Pillot, J.-P. Route to Smooth Silica-Based Surfaces Decorated with Novel Self-Assembled Monolayers (SAMs) Containing Glycidyl-Terminated Very Long Hydrocarbon Chains. *Langmuir* **2009**, *25* (10), 5526–5535. https://doi.org/10.1021/la804088d.

(34) Palazon, F.; Montenegro Benavides, C.; Léonard, D.; Souteyrand, É.; Chevolot, Y.; Cloarec, J.-P. Carbodiimide/NHS Derivatization of COOH-Terminated SAMs: Activation or Byproduct Formation? *Langmuir* **2014**, *30* (16), 4545–4550. https://doi.org/10.1021/la5004269.

(35) Holzweber, M.; Heinrich, T.; Kunz, V.; Richter, S.; Traulsen, C. H.-H.; Schalley, C. A.; Unger, W. E. S. Principal Component Analysis (PCA)-Assisted Time-of-Flight Secondary-Ion Mass Spectrometry (ToF-SIMS): A Versatile Method for the Investigation of Self-Assembled Monolayers and Multilayers as Precursors for the Bottom-Up Approach of Nanoscaled Devices. *Anal. Chem.* **2014**, *86* (12), 5740–5748. https://doi.org/10.1021/ac500059a.

(36) Hill, J. M.; Royce, D. G.; Fadley, C. S.; Wagner, L. F.; Grunthaner, F. J. Properties of Oxidized Silicon as Determined by Angular-Dependent X-Ray Photoelectron Spectroscopy. *Chemical Physics Letters* **1976**, *44* (2), 225–231. https://doi.org/10.1016/0009-2614(76)80496-4.

(37) Ofir, Y.; Zenou, N.; Goykhman, I.; Yitzchaik, S. Controlled Amine Functionality in Self-Assembled Monolayers via the Hidden Amine Route: Chemical and Electronic Tunability. *J. Phys. Chem. B* **2006**, *110* (15), 8002–8009. https://doi.org/10.1021/jp057251k.

(38) James, M.; Darwish, T. A.; Ciampi, S.; Sylvester, S. O.; Zhang, Z.; Ng, A.; Gooding, J. J.; Hanley, T. L. Nanoscale Condensation of Water on Self-Assembled Monolayers. *Soft Matter* **2011**, *7* (11), 5309–5318. https://doi.org/10.1039/C1SM05096F.

(39) Artemenko, A.; Shchukarev, A.; Štenclová, P.; Wågberg, T.; Segervald, J.; Jia, X.; Kromka, A. Reference XPS Spectra of Amino Acids. *IOP Conf. Ser.: Mater. Sci. Eng.* **2021**, *1050* (1), 012001. https://doi.org/10.1088/1757-899X/1050/1/012001.

(40) Böhmler, J.; Ponche, A.; Anselme, K.; Ploux, L. Self-Assembled Molecular Platforms for Bacteria/Material Biointerface Studies: Importance to Control Functional Group Accessibility. *ACS Appl. Mater. Interfaces* **2013**, *5* (21), 10478–10488. https://doi.org/10.1021/am401976g.

(41) Ma, Z.; Tian, L.; Qiang, H. A Facile Approach for Self-Assembled Gold Nanorods Monolayer Films and Application in Surface-Enhanced Raman Spectroscopy. *J. Nanosci. Nanotech.* **2009**, *9* (11), 6716–6720. https://doi.org/10.1166/jnn.2009.1365.

(42) Orendorff, C. J.; Gole, A.; Sau, T. K.; Murphy, C. J. Surface-Enhanced Raman Spectroscopy of Self-Assembled Monolayers: Sandwich Architecture and Nanoparticle Shape Dependence. *Anal. Chem.* **2005**, *77* (10), 3261–3266. https://doi.org/10.1021/ac048176x.

(43) Pekcevik, I. C.; Poon, L. C. H.; Wang, M. C. P.; Gates, B. D. Tunable Loading of Single-Stranded DNA on Gold Nanorods through the Displacement of Polyvinylpyrrolidone. *Anal. Chem.* **2013**, *85* (20), 9960–9967. https://doi.org/10.1021/ac4027737.

(44) Wu, J.; Qu, Y.; Yu, Q.; Chen, H. Gold Nanoparticle Layer: A Versatile Nanostructured Platform for Biomedical Applications. *Mater. Chem. Front.* **2018**, *2* (12), 2175–2190. https://doi.org/10.1039/C8QM00449H.

(45) Itoh, T.; Kikkawa, Y.; Biju, V.; Ishikawa, M.; Ikehata, A.; Ozaki, Y. Variations in Steady-State and Time-Resolved Background Luminescence from Surface-Enhanced Resonance Raman Scattering-Active Single Ag Nanoaggregates. *J. Phys. Chem. B* **2006**, *110* (43), 21536–21544. https://doi.org/10.1021/jp064070p.

(46) Pettinger, B.; Domke, K. F.; Zhang, D.; Schuster, R.; Ertl, G. Direct Monitoring of Plasmon Resonances in a Tip-Surface Gap of Varying Width. *Phys. Rev. B* **2007**, *76* (11), 113409. https://doi.org/10.1103/PhysRevB.76.113409.

(47) Mayer, K. M.; Hafner, J. H. Localized Surface Plasmon Resonance Sensors. *Chem. Rev.* **2011**, *111* (6), 3828–3857. https://doi.org/10.1021/cr100313v.

(48) Garcia-Rico, E.; Alvarez-Puebla, R. A.; Guerrini, L. Direct Surface-Enhanced Raman Scattering (SERS) Spectroscopy of Nucleic Acids: From Fundamental Studies to Real-Life Applications. *Chem. Soc. Rev.* **2018**, *47* (13), 4909–4923. https://doi.org/10.1039/C7CS00809K.

(49) Safar, W.; Azziz, A.; Edely, M.; Lamy de la Chapelle, M. Conventional Raman, SERS and TERS Studies of DNA Compounds. *Chemosensors* **2023**, *11* (7), 399. https://doi.org/10.3390/chemosensors11070399.